INTERNATIONAL JOURNAL OF AUTOMOTIVE AND MECHANICAL ENGINEERING
ISSN: 2229-8649 e-ISSN: 2180-1606
VOLUME 22, ISSUE 2, 2025, 12468 - 12482
DOI: https://doi.org/10.15282/ijame.22.2.2025.16.0953

RESEARCH ARTICLE

Selection of Intrinsic Mode Functions Using Statistical Indicators for Knock Detection in Spark-Ignition Engines

Antonio Joseph V K*, Gireesh Kumaran Thampi

Department of Mechanical Engineering, School of Engineering, Cochin University of Science and Technology, 682022 Kalamassery, India

ABSTRACT – Spark-ignition (SI) engine knock remains a critical challenge that adversely affects engine performance, efficiency, and durability. Real-time knock detection using engine block vibration signals is complex due to its nonlinear and non-stationary nature. Advanced signal decomposition techniques such as Empirical Mode Decomposition (EMD), Ensemble Empirical Mode Decomposition (EEMD), Complete Ensemble Empirical Mode Decomposition with Adaptive Noise (CEEMDAN), and Variational Mode Decomposition (VMD) are commonly employed to extract knock-related features. However, there is limited consensus on selecting the intrinsic mode functions (IMFs) that best represent knock characteristics. This work introduces a statistical selection criterion based on correlation coefficient (> 0.5), approximate entropy (ApEn > 0.5), and kurtosis (two IMFs with the highest kurtosis values) to identify knock-relevant IMFs. Vibration signals were denoised using Symlet wavelets and then decomposed using the aforementioned techniques. The effectiveness of the selection was evaluated using spectrogram analysis and validated with Maximum Amplitude of Pressure Oscillation (MAPO) values. Results demonstrate that the proposed selection criteria successfully isolated knock-related IMFs, particularly IMF1 and IMF2 when CEEMDAN was applied to signals at 4000 rpm - an improvement over previous works in which only IMF1 was considered for knock analysis. The selected IMFs corresponded to MAPO values exceeding 2 bars, confirming strong knock events. Higher ApEn values, approaching 1 for IMF1 of the vibration signal at 4000 rpm, may be attributed to two strong knock events (cylinders 2 and 3). In contrast, ApEn values around 0.6 for IMF1 at 2800 rpm corresponding to one strong knock (cylinder 1) and one weak knock (cylinder 3) suggest that further investigation is required to confirm the correlation between approximate entropy and knock intensity. This multi-metric approach enhances the robustness and reliability of knock detection and offers a low-complexity, high-accuracy framework suitable for real-time implementation using non-intrusive vibration sensors.

ARTICLE HISTORY

Received : 26th June 2024
Revised : 05th May 2025
Accepted : 21st May 2025
Published : 27th June 2025

KEYWORDS

SI engine
Knocking
Approximate entropy
Kurtosis
Correlation coefficient

1. INTRODUCTION

Spark-ignition engine knock remains one of the most critical challenges in modern engine design, as it directly limits thermal efficiency, power output, and durability. The phenomenon occurs due to the auto-ignition of the unburned air-fuel mixture in the end-gas region ahead of the propagating flame front, often triggered by high in-cylinder pressures and temperatures [1, 2]. Despite advancements in knock suppression methods, accurately detecting knock in real-time continues to be essential for optimizing combustion phasing, maximizing performance, and avoiding engine damage. This study seeks to deliver an in-depth and analytical assessment of knock detection methods, focusing on signal decomposition methods and statistical feature extraction techniques for real-time knock identification. One of the most influential variables in knock formation is the ignition strategy. Multiple spark ignitions are used to reduce the knock's intensity or suppress it [3]. Although multiple spark ignition can initially increase knock due to faster combustion, it has been observed that the overall knock intensity is reduced with four spark plugs—likely due to a more complete and uniform combustion that limits unburned end-gas mass [3]. This is because the greater the number of spark plugs used, the less energy remains for knock to occur, further suppressing it [4]. Another type of knock suppression method is the use of prechamber. Knock-limited combustion phasing is significantly extended with the prechamber ignition [5].

In addition to the ignition strategy, fuel blends can also be used to reduce the possibility of knock occurrence and improve engine performance [6]. Co-injection of a water-methanol blend is seen to improve the SI engine's thermal efficiency and reduce the knock tendency and cycle-to-cycle variation more effectively [7]. Water injection is another method used to reduce the temperature of charge inside the cylinder, reducing the occurrence of knock [8, 9]. Another method is the use of cooled EGR [10]. This could dilute the fresh charge, thereby reducing its temperature and advancing the knock limit [10]. Even though many methods are available for preventing or delaying the occurrence of knock, improved performance could be achieved only by detecting and controlling knock in real-time.

***CORRESPONDING AUTHOR | Antonio Joseph V K |** ✉ antoniojosephvk@gmail.com

1.1 Knock Detection Techniques

To complement preventive measures, real-time detection and mitigation of knock remain essential. Several signal sources are employed for knock detection, including in-cylinder pressure, localized heat transfer at the cylinder walls, acoustic signals, ionization in the air-fuel mixture, and engine block vibration [11–15]. In-cylinder pressure measurements are frequently employed for knock detection owing to their superior signal-to-noise ratio, which offers greater detection accuracy compared to engine block vibration signals [14]. However, mounting the pressure transducers may weaken the combustion chamber, hence its use is mainly limited to research/laboratory purposes. However, efforts are being made to develop a non-intrusive pressure sensor. Corti et al. [16] integrated a non-intrusive pressure sensor into the spark plug to achieve accurate knock detection. They noted that the vibrations associated with the engine parts located near the spark plug and higher temperature affect the sensor readings, leading to a reduced signal-to-noise ratio [16]. Another option is the use of accelerometers. However, vibration signals have a much lower signal-to-noise ratio and show a greater dependence on the position at which it is mounted on the engine [17]; it is still an ideal choice due to its practical feasibility. The low cost of the sensor, ease of mounting it, easier maintenance, and ease of integration with ECU or IoT for real-time monitoring makes it an ideal choice [14]. Vibration sensors are non-intrusive also.

Nevertheless, the lower signal-to-noise ratio necessitates effective pre-processing, feature extraction, and the development of robust analytical models to enhance detection accuracy. The amplitude of vibrations generated during knock events can vary from one engine cycle to another. The amplitudes will be higher if the knock occurs at the early stages of combustion due to the large number of unburnt masses available, while the amplitude will be lower at the later stages. Hence, Pla et al. [18] used a combustion model to estimate the mass fraction burnt corresponding to the vibration signals obtained. However, this could not be implemented for real-time monitoring due to the requirement of combustion models for the entire range of operating conditions. Additionally, the non-uniformity of the spatial pattern of knock also leads to the fluctuation in the engine block vibrations for the same knock intensity. Thermal conditions, as well as the composition of the mixture inside the combustion chamber, affect the spatial distribution of the knock [4, 19]. Within these limitations, robust models should be developed to analyze vibration signals and determine the occurrence of knock in real-time. The model thus developed should be computationally efficient while maintaining high accuracy. Many research studies have already been conducted, and ongoing efforts continue to enhance the robustness and accuracy of these models.

1.2 Signal Decomposition Methods

Various signal decomposition methods have been developed to handle the complex nature of vibration signals, which are inherently non-linear and non-stationary. These include techniques such as Discrete Wavelet Transform (DWT), Empirical Mode Decomposition (EMD), Ensemble EMD (EEMD), Complete Ensemble EMD with Adaptive Noise (CEEMDAN), and Variational Mode Decomposition (VMD), all of which are designed to extract meaningful signal components from noisy or complex datasets. One of the most commonly used techniques is the Discrete Wavelet Transform (DWT), which decomposes signals into multiple frequency bands [20]. Sharp spikes in the energy of the D1 (high-frequency component of the signal) band may indicate knock events; however, they can also result from other high-frequency phenomena, such as mechanical noise or valve train vibrations. Therefore, additional validation is necessary. However, DWT is an ideal choice for real-time analysis due to its faster computation and robustness [20]. However, its reliance on fixed wavelet bases may limit adaptability for more complex signals.

In contrast, Empirical Mode Decomposition (EMD) is more effective for in-depth analysis where signal complexity demands adaptive techniques. The signals decompose into Intrinsic Mode Functions (IMFs) with slowly varying amplitude and phase [21]. EMD generates components that are locally modulated in both amplitude and frequency, while also being data-driven and exhibiting sparse representations [21, 22]. This allows the method to extract inherent signal features across various scales without relying on predefined assumptions like harmonic, non-stationary, etc., as is done while performing wavelet Transform or Fourier analysis [23, 24]. Thus, the IMFs obtained have inter-wave and intra-wave frequency modulations [21]. However, EMD often suffers from mode mixing and lacks robustness when applied to signals with overlapping frequency content, which makes its output sensitive to signal noise.

EEMD enhances the standard EMD by introducing white Gaussian noise, which helps mitigate mode mixing issues by leveraging EMD's dyadic filter bank characteristics [25, 26]. A better signal-to-noise ratio can also be achieved with the addition of white noise [27]. However, it leads to a different number of IMFs than the actual number of modes present in the original signal [28]. Also, the IMFs that were obtained may have residues of the white noise that was added [29]. In addition, the ensemble number and the noise standard deviation need to be specified before the analysis; hence, it is not adaptive as an EMD. This led to the introduction of an improved version called Complete Ensemble Empirical Mode Decomposition (CEEMD) [28], which calculates the local mean curve to decompose the original signal into different modes having apparent physical meaning [30]. Due to the presence of complementary pairs of noise in the different modes obtained, perfect reconstruction of the original signal was impossible [31]. This issue was addressed by CEEMDAN, which is an improved version of CEEMD with the addition of adaptive noise to the original signal [29]. CEEMDAN can be used to produce better spectral separation of modes.

In contrast to these decomposition methods, VMD is an entirely non-recursive approach that simultaneously extracts all modes. VMD is well-suited for analyzing complex, non-linear, and non-stationary signals. VMD demonstrates superior performance over EMD in terms of identifying distinct tones, effectively separating them, and noise robustness [32]. This is due to its self-optimization and adaptive usage of the Wiener filter. Even though this is the case, VMD requires explicit selection of the number of modes of decomposition that need to be achieved, as opposed to EMD [33]. Therefore, if the number of modes is chosen wrongly, it may lead to the loss of some important modes or result in mixing different modes [34]. The most advanced methods include the use of wavelet decomposition, or the EMD family, to decompose the signals [35] and use Artificial Neural Networks (ANN), Deep Learning Convolutional Neural Networks (DLCNN) etc. for extracting the features of knock obtained to distinguish between non-knock and knock cycles [14, 23, 36, 37]. However, the requirement of training the datasets and the higher computational power required are its drawbacks for real-time detection.

1.3 Statistical Feature-Based Knock Identification

Feature extraction plays a critical role in distinguishing knock events from normal combustion, particularly when used along with signal decomposition techniques. While methods such as EMD, EEMD, CEEMDAN and VMD have been widely applied to extract knock-related features, their performance heavily depends on the accurate identification of knock-relevant IMFs. However, most existing approaches lack systematic selection criteria and often depend on manual interpretation or heuristic thresholds, limiting their reliability in real-time applications. To address this gap, the present work proposes a systematic IMF selection criterion based on a combination of statistical tools. This multi-feature strategy could reduce subjectivity, improve consistency, and lower computational complexity—making it well-suited for real-time knock detection without the need for complex classification models.

There are many statistical tools like Multi-scale Permutation Entropy [38], kurtosis [39], approximate entropy [40], correlation coefficient [22], and tools used in fractal analysis like Hurst exponent, fractal dimension, multifractal spectrum etc. [41]. Among these, the fractal analysis provides valuable insights into combustion instability and detects the transition from stable to unstable combustion, but it is computationally complex [41]. Due to its computational complexity, fractal analysis is currently more suited for offline analysis than real-time knock control unless optimized algorithms or high-speed computation facilities are employed. Multi-scale Permutation Entropy (MPE) is a feature extraction method that is best suited for non-linear noisy signals [38]. MPE can detect both fast and sudden knock and slower and evolving knock patterns by analyzing the vibration signal at multiple resolutions. However, approximate entropy is simpler and, requires less computational time and is best suited for the quick identification of knock events. Approximate entropy can also produce even better results if combined with other statistical features like kurtosis.

Prior studies have explored IMF-based knock detection using EMD-family methods, Hilbert transforms, wavelet filtering [23], and deep learning-based classification [36, 37]. However, these approaches suffer from either reliance on manual IMF selection, computationally intensive training requirements, or limited real-time applicability. Studies show that the wavelet and ANN-based classifiers offer good accuracy but lack interpretability and generalizability across engine types and operating conditions [23]. Apart from these, the present work introduces multi-feature statistical selection criteria using correlation coefficient, approximate entropy, and kurtosis, allowing automated, objective-oriented, and reproducible identification of IMFs that contain the signals produced during knock. This method is computationally efficient and can be extended to real-time applications without any trained data. The selection criteria proposed in the current work are validated using Maximum Amplitude of Pressure Oscillation (MAPO) values. MAPO of the in-cylinder pressure signals that correspond to the engine block vibrations are also used to classify the combustion process occurring in each cylinder as non-knock (MAPO below 0.5 bar), weak knock (0.5–2 bar) and strong knock (above 2 bar) cycles [42].

In the current work, the engine block vibrations recorded are decomposed using EMD, EEMD, CEEMDAN, and VMD. Thus, the correlation coefficient, approximate entropy, and kurtosis of the IMFs that were obtained are calculated. Considering these values, a selection criterion is proposed to choose the IMFs that may contain the signals produced during the knock. The IMFs satisfying the selection criterion are analyzed further to obtain the spectrogram. The efficacy of the proposed selection criteria in choosing the IMFs containing the knock features is also evaluated. Further details about the selection criteria and its evaluation are discussed in the following sections.

2. SIGNAL ANALYSIS AND SELECTION OF INTRINSIC MODES

The vibration datasets used in the current analysis are sourced from the works of Fengrong et al. [43, 44] and Li et al. [45]. They had produced knock by advancing the ignition timing of a 4-cylinder, 4-stroke in-line SI engine. The signals are captured using the accelerometers DYTRAN-621B40 [43 – 45], mounted on the engine block. In-cylinder pressure signals are captured using AVL - GH13Z-31(24) [43 – 45]. These datasets were selected due to their high-quality simultaneous recordings of engine block vibrations and in-cylinder pressure, along with documented knock-inducing operating conditions, which are ideal for validating decomposition and IMF selection criteria. Noise contained in the vibration signal is eliminated using the Symlet wavelet due to its better symmetry, thereby reducing the chance of phase distortion. Soft thresholding is used to avoid discontinuities in the denoised signal [46]. After denoising, the signals are decomposed using EMD, EEMD, CEEMDAN, and VMD. For VMD, the number of modes was set to 6, which provides a balance between the decomposition resolution and computational efficiency for vibration signal analysis [47]. In the case of CEEMDAN, the noise amplitude was set to 0.2 and the ensemble size to 100, based on reported values in the work done by Morteza et al. [48]. These values offer a reliable trade-off between noise robustness and decomposition accuracy. The IMFs obtained after decomposition are then evaluated to find their correlation coefficient with the original signal, approximate entropy, and kurtosis. The correlation coefficient could be used to identify the IMF that is more similar to the original signal. In contrast, approximate entropy and kurtosis can be used to identify the IMFs with higher amplitude signals or spikes concentrated at a few points in a time series. On the other hand, the remaining part of the signal remains almost flat. These could effectively identify the high frequency, high amplitude engine block vibration signals that are induced by the engine knock.

2.1 Correlation Coefficient

The correlation coefficient ρ, measures the similarity between two signals. Signals show a strong correlation when the value is nearer to 1 or -1 and the least correlation when the value is closer to 0 [22]. Since the knock causes vibrations with a higher frequency and amplitude, IMFs with a high correlation to the original signal may contain dominant vibration components, including those related to knock or other recurring combustion dynamics. Hence, the correlation coefficient alone cannot definitely identify knock and must be used along with other features.

The correlation coefficient is calculated using the relation [49]:

$$\rho = \frac{\sum_{i=1}^{N}(X_i - \mu_X)\,(Y_i - \mu_Y)}{\left(\sqrt{\sum_{i=1}^{N}(X_i - \mu_X)^2}\right)\left(\sqrt{\sum_{i=1}^{N}(Y_i - \mu_Y)^2}\right)} \tag{1}$$

Here, X and Y are the set of variables to be compared, N is the number of observations, μ_X and μ_Y are the arithmetic mean of the set of variables X and Y.

The arithmetic mean of the variables is calculated as [49],

$$\mu_X = \frac{\sum_{i=1}^{N} X_i}{N} \tag{2}$$

$$\mu_Y = \frac{\sum_{i=1}^{N} Y_i}{N} \tag{3}$$

2.2 Approximate Entropy

Approximate entropy (ApEn), proposed by Pincus [50], quantifies the irregularities present in time-series data [50]. ApEn of time-series data is obtained as a non-negative value, with higher values representing more irregularity and complexity of the data/signal, while values close to zero denote a more regular pattern of the data/signal [40]. Hence, periodic data with a single frequency component will have low ApEn values, while a complex signal with multiple frequency components will have high ApEn values. Higher ApEn values indicate increased signal complexity or irregularity, which may also be associated with knock events. However, such complexity may also arise from other transient phenomena, so ApEn alone could not produce the desired results.

For a given N data points in the signal data $u(i)$, approximate entropy is calculated as follows [50]:

Initially, the m vector sequences $X(1) \ldots\ldots X(N-m+1)$ of the time-series data $u(i)$ are formed as,

$$X(i) = [u(i), u(i+1), \ldots\ldots\ldots u(i+m-1)] \tag{4}$$

where, $1 \le i \le N - m + 1$

The distance between the vectors, $X(i)$ and $X(j)$, i.e., the maximum difference in their scalar components, is calculated as [50],

$$d[X(i), X(j)] = \max_{k=1,\ldots\ldots m}(|x(i+k)x(j+k)|) \tag{5}$$

The frequency of similar patterns $C_r^m(i)$ measured for the vector sequences $X(i)$ is [50],

$$C_r^m(i) = \frac{N^m(i)}{N - m + 1} \tag{6}$$

The approximate entropy of the signal is then calculated using the relation [50],

$$ApEn = \Phi^m(r) - \Phi^{m+1}(r) \tag{7}$$

Here, r is a tolerance value (generally taken between 0.01 and 0.5) and $\Phi^m(r) = \frac{1}{N-m+1}\sum_{i=1}^{N-m+1} \ln C_r^m(i)$.

$N^m(i)$ counts the number of j satisfying the condition $d[X(i), X(j)] \le r$ while the value range for j will be $1 \le j \le N - m + 1$.

2.3 Kurtosis

Kurtosis represents the measure of flattening of the probability density function near the mean value of the signal [39]. Therefore, the pulse nature of the signal can be represented using kurtosis [39]. In other words, kurtosis measures the peakedness of the signal [39]. Generally, the pulse signal will have a kurtosis value higher than 3. Moreover, a higher kurtosis value means more peaks in the signal, having more than 3 times the RMS value of the signal [39]. For a sample of n values, $u_1, u_2 \ldots . u_n$, kurtosis is calculated using the formula [39],

$$k = \left[\frac{n(n+1)}{(n-1)(n-2)(n-3)}\sum_{i=1}^{n}\left(\frac{u_i-\bar{u}}{s}\right)^4\right] - \frac{3(n-1)^2}{(n-2)(n-3)} \tag{8}$$

Kurtosis can be further categorized as:

- **Positive kurtosis (leptokurtic):** This describes a distribution with fatter tails than a normal distribution, indicating that there are more outliers than the norm in both directions (higher and lower values).
- **Negative kurtosis (platykurtic):** This describes a distribution in which there are fewer outliers than the norm and thinner tails than in a normal distribution.
- **Kurtosis of zero (mesokurtic):** This indicates a distribution with tails similar in size to those of a normal distribution with a moderate frequency of outliers.

Vibration signals affected by knock often exhibit a leptokurtic distribution due to the presence of sharp peaks. However, the distribution shape can vary depending on combustion conditions and the engine's operating state.

2.4 Criteria for Choosing the IMF

The proposed selection criteria for choosing the IMFs that may contain the signals generated during the knock are as follows:

- IMFs with a correlation coefficient greater than 0.5 with the original signal can be selected.
- IMFs with approximate entropy (ApEn) above 0.5 can be selected. This is because the IMFs that contain the vibration signals produced during knock will have higher ApEn values. This is due to the presence of high-frequency, high-amplitude signals.
- Since kurtosis depends on the RMS value of each signal and the amplitudes of peaks present in the corresponding signal, general criteria cannot be made for selecting the IMFs. This is because the IMFs with comparatively lower peaks but much lower RMS values may have higher kurtosis than those with higher peaks, such as those produced during the occurrence of knock, which have a much higher RMS value than the former. Therefore, two IMFs with the highest kurtosis value can be selected instead of providing a threshold value.

The IMFs satisfying all three criteria are then further analyzed to generate a spectrogram that can be used to identify the specific cylinder where knock events are detected. The energy distribution in a time-frequency domain obtained in the spectrogram could easily locate the high amplitude, high-frequency vibrations (if any) on a time scale. This, along with the signal from the crank position sensor, facilitates precise identification of the cylinder experiencing a knock. However, if the knock occurs due to the lean air-fuel mixtures, higher compression ratios, engine heating, spark timing, etc., which affect the entire engine, there is no point in identifying the specific cylinder where knock events occur. Preventive measures are required for all cylinders. If the knock occurs due to the hot spots inside the combustion chamber caused by carbon deposits, the control mechanism is to clean the combustion chamber. This should be done manually. In short, rather than locating the cylinder, real-time detection of the knock and its control or preventing its further occurrence is required. The selection criteria proposed in the current work could be used to detect the occurrence of knock. The correlation coefficient, approximate entropy, and kurtosis values calculated for each IMF were evaluated to substantiate the effectiveness of the proposed selection criteria.

3. RESULTS AND DISCUSSION

3.1 Selection of IMFs

The engine block vibrations reflecting the knock events were recorded while the engine was running at 4000 rpm with a spark at 20° BTDC and 2800 rpm with a spark at 28° BTDC, respectively [45], are decomposed using EMD, EEMD, VMD, and CEEMDAN. Tables 1 and 2 show the correlation coefficient, approximate entropy, and kurtosis values calculated for each IMF thus obtained. IMFs satisfying the selection criteria discussed in section 2.4 are highlighted in green, while those satisfying at least any one of the three criteria are highlighted in yellow. The values calculated show that the first IMF obtained using EMD, EEMD, and CEEMDAN met the selection criteria, while none of the IMFs obtained using VMD could meet the selection criteria. The second IMF obtained using CEEMDAN (Table 1) also satisfies the selection criterion. This suggests that EMD, EEMD, and CEEMDAN can effectively capture high-frequency components potentially associated with knock events from the engine block vibration signals. However, further analyses of the selected IMFs are required to confirm the same observation.

Table 1. Correlation coefficient, approximate entropy, and kurtosis calculated for each IMF obtained after performing EMD, EEMD, CEEMDAN, and VMD on the engine block vibration signal obtained at 4000 rpm [45]

	IMF 1	IMF 2	IMF 3	IMF 4	IMF 5	IMF 6	IMF 7	IMF 8
				Correlation Coefficient				
EMD	0.92	0.25	0.08	0.018	0.02	-0.001	0.006	0.005
EEMD	0.80	0.86	0.42	0.260	0.10	0.046	0.040	0.018
CEEMDAN	0.84	0.58	0.70	0.380	0.24	0.090	0.035	0.030
VMD	0.18	0.26	0.49	0.730	0.45	0.330		
				Approximate Entropy				
EMD	1.02	0.62	0.45	0.25	0.11	0.04	0.02	0.009
EEMD	0.99	0.82	0.67	0.58	0.48	0.22	0.10	0.040
CEEMDAN	0.84	0.61	0.90	0.66	0.57	0.55	0.30	0.140
VMD	0.32	0.42	0.43	0.38	0.56	0.60		
				Kurtosis				
EMD	5.99	10.27	5.74	5.076	2.84	2.156	2.21	2.028
EEMD	13.49	3.70	5.78	4.020	3.45	3.230	2.32	2.018
CEEMDAN	9.35	29.76	3.19	6.570	4.23	2.880	4.57	2.510
VMD	43.99	13.48	5.13	5.290	3.79	4.800		

Table 2. Correlation coefficient, approximate entropy, and kurtosis calculated for each IMF obtained after performing EMD, EEMD, CEEMDAN, and VMD on the engine block vibration signal obtained at 2800 rpm [45]

	IMF 1	IMF 2	IMF 3	IMF 4	IMF 5	IMF 6	IMF 7	IMF 8
				Correlation Coefficient				
EMD	0.92	0.31	0.09	0.007	0.008	0.019	0.003	0.003
EEMD	0.80	0.71	0.34	0.20	0.04	0.02	0.03	0.023
CEEMDAN	0.82	0.47	0.53	0.26	0.17	0.028	0.01	0.02
VMD	0.27	0.46	0.47	0.67	0.43	0.27		
				Approximate Entropy				
EMD	0.64	0.36	0.36	0.22	0.09	0.04	0.02	0.007
EEMD	0.54	0.57	0.54	0.37	0.45	0.17	0.10	0.04
CEEMDAN	0.54	0.78	0.94	0.71	0.40	0.48	0.22	0.15
VMD	0.38	0.29	0.34	0.33	0.44	0.33		
				Kurtosis				
EMD	24.73	20.9	17.3	9.2	8.45	2.5	2.65	1.5
EEMD	45.77	14.97	15.54	9.48	5.05	8.86	4.02	2.53
CEEMDAN	34.51	62.75	8.44	26.96	10.02	8.40	10.38	4.08
VMD	40.77	29	11.8	13.3	14.2	13.88		

The results also show that none of the IMFs obtained using VMD satisfied the selection criteria. This may indicate a limitation of VMD for knock detection under the given conditions. Unlike other methods, VMD decomposes the signal into narrowband IMFs that are concentrated around specific center frequencies. This characteristic may not be suitable for capturing non-linear and non-stationary engine block vibrations produced during SI engine knock, with frequencies ranging from 7 kHz to 22 kHz. VMD might have distributed the knock-related information across multiple narrowband IMFs, failing to represent the spikes or sharp rise in the amplitudes of vibration signals in a single IMF. The spectrogram of the IMFs obtained using VMD should be evaluated before reaching a final conclusion regarding the effectiveness of VMD in detecting the signals produced during SI engine knock.

The proposed multi-metric selection approach enhances reliability and repeatability, as opposed to the methods that rely on visual inspection of spectrograms [44–46] and single-feature analysis such as kurtosis [39]. Some other works used ANN, DLCNN etc. [14, 23, 36, 37] to detect a knock but lacked interpretability and real-time feasibility. Our approach achieves comparable accuracy without requiring machine learning training data and with much lower computation. To validate these observations, spectrograms were generated for all IMFs obtained using each decomposition method (EMD, EEMD, VMD, and CEEMDAN). The spectrograms were then visually inspected to identify IMFs that clearly demarcate the occurrence of knocking events. These results are compared with the IMFs selected based on the above-mentioned selection criteria to further evaluate their effectiveness in knock detection. Further details regarding the spectrogram of the IMFs obtained, the effectiveness of the selection criteria, and the effectiveness of each decomposition method in identifying the occurrence of knock are discussed in the following sections.

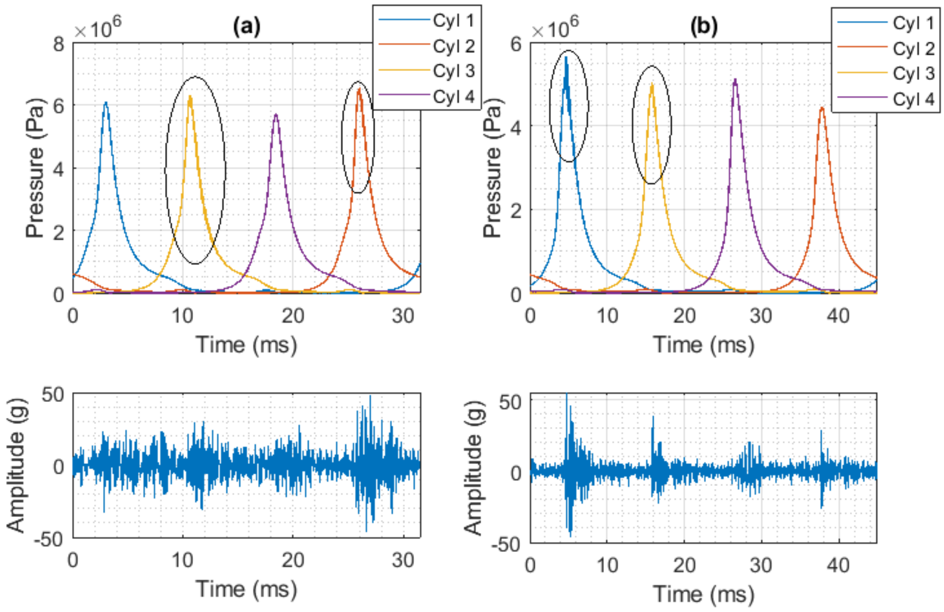

Figure 1. In-cylinder pressure and engine block vibrations produced by the engine running at (a) 4000 rpm, spark at 20° BTDC, and (b) 2800 rpm, 28° BTDC [45]

3.2 Analysis of IMFs

Figures 1(a) and (b) show the in-cylinder pressure and engine block vibrations produced by the engine running at 4000 rpm with a spark at 20° BTDC and 2800 rpm with a spark at 28° BTDC, respectively [45]. In Figure 1(a), pressure fluctuations are observed in the in-cylinder pressure values corresponding to the combustion process in cylinders 2 and 3. These may be due to the occurrence of knock. MAPO corresponding to the combustion process in cylinders 1-4 is calculated to be 0.46 bar, 2.12 bar, 2.15 bar, and 0.43 bar, respectively. From the MAPO calculated, it is clear that a strong knock occurs in cylinders 2 and 3, while non-knocking cycles are observed in cylinders 1 and 4. Higher amplitude engine block vibration signals are visible in line with pressure fluctuations produced in cylinder 2. However, such high amplitude vibration signals are not observed, corresponding to the pressure fluctuations produced inside cylinder 3. Therefore, it is inferred that, based solely on the amplitudes of the engine block vibration signals, a conclusion regarding the occurrence of knock cannot be made. Similar to that seen in Figure 1(a), pressure fluctuations are observed in the in-cylinder pressure values corresponding to the combustion process in cylinders 1 and 3 in Figure 1 (b). MAPO is calculated to be 4.94 bar, 0.18 bar, 1.93 bar, and 0.28 bar, corresponding to the combustion process in cylinders 1–4, respectively, indicating a strong knock in the first cylinder, a weak knock in the third cylinder, and a non-knocking cycle in the remaining two cylinders. From Figure 1(b), it is also observed that the peak pressure produced during the combustion process in cylinder 1 is higher than that produced during the combustion process inside cylinder 3. Similarly, the pattern of vibration signals is also.

However, vibrations produced in the latter case also exhibit higher amplitudes when compared to the vibration signals produced corresponding to the combustion process inside cylinders 2 and 4 (non-knocking cycles). However, the vibrations produced during the combustion process inside cylinder 2 also have some peaks, even though they are not as high as those produced during the combustion process inside cylinders 1 and 3. However, the fluctuations in the in-cylinder pressure aren't evident during the combustion process occurring in cylinder 2. Therefore, it might not be caused by the knock. Higher amplitude vibrations may also be produced due to other factors. Based on the vibration signals recorded at engine speeds of 2800 rpm and 4000 rpm, it can be inferred that the amplitude of combustion-induced vibrations, by itself, is insufficient to indicate the presence of knock reliably. Other parameters like valve opening and closing, misfire, spark timing, the equivalence ratio of the air-fuel mixture, etc., will also affect the amplitude of the vibrations produced. Hence, the vibration signals obtained need to be processed further to observe them in a time-frequency domain to get more details regarding their frequency distribution. This, in turn, could identify the high frequency, high amplitude vibration signals that correspond to the one that is produced during the knock.

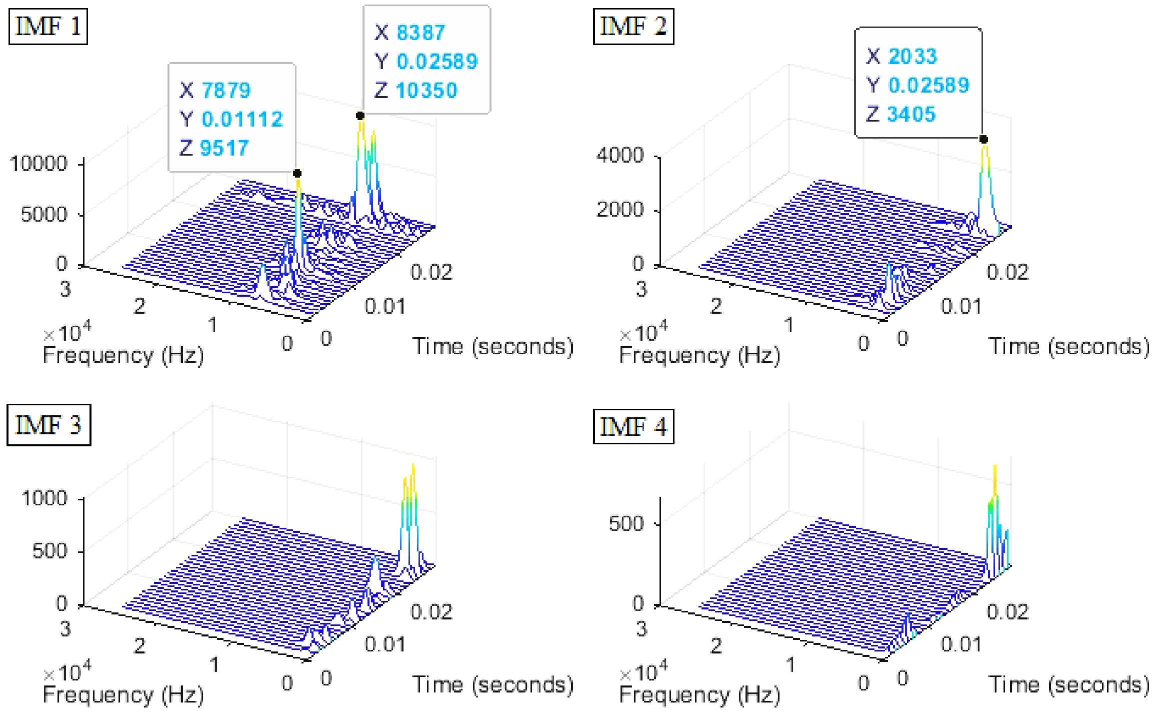

Figure 2. Spectrograms of the first four IMFs extracted using EMD from vibration signals recorded at 4000 rpm and spark at 20° BTDC

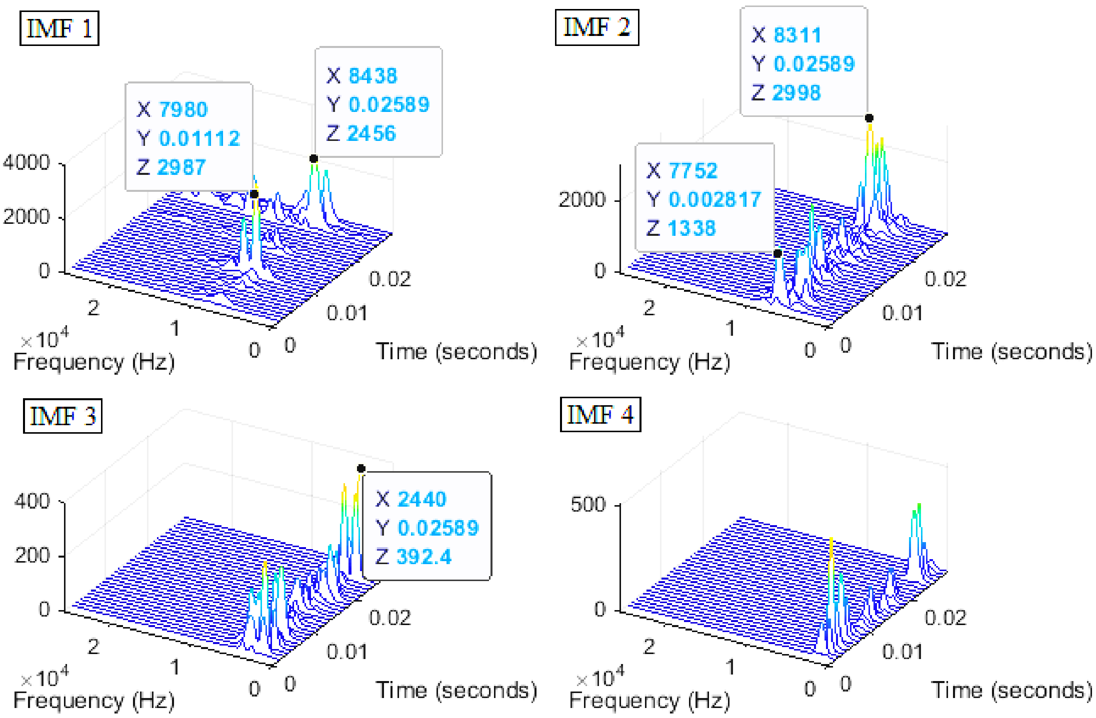

Figure 3. Spectrograms of the first four IMFs extracted using EEMD from vibration signals recorded at 4000 rpm and spark at 20° BTDC

The spectrogram of IMFs obtained by decomposing the engine block vibrations captured from the engine at 4000 rpm and spark at 20° BTDC is shown in Figures 2-5 [45]. The signals are decomposed using EMD, EEMD, CEEMDAN, and VMD, respectively. Figure 2 shows the spectrogram of the first four IMFs obtained using EMD. The results show that higher energy fluctuations are present only in the first IMF, at 0.01112 seconds and 0.02589 seconds, respectively. This corresponds to the combustion process occurring inside cylinders 3 and 2. The first peak observed at 0.01112 seconds has a frequency of 7879 Hz, while the second peak observed at 0.02589 seconds has a frequency of 8387 Hz. These higher energies are observed between 7 and 22 kHz; knock-induced engine block vibrations generally fall in this range. The pressure fluctuations and the MAPO calculated also confirm the same. The maximum energy of the remaining IMFs is observed to have a frequency below 2 kHz. Therefore, from the results, it is clear that only the first IMF contains the components of the signal produced during the SI engine knock. The same was also observed using the proposed selection criteria (section 2.4).

Figure 3 shows the spectrogram of IMFs obtained by decomposing the signals using EEMD. The results show that signals with a frequency above 7 kHz are present in both the first and second IMFs. However, the second IMF fails to provide a clear demarcation about the occurrence of a knock since the signals having frequencies around 7 kHz are found throughout the signal length. Hence, it is evident that the vibrations, which have frequencies around 7 kHz, are produced by the engine during the normal combustion cycles as well. Therefore, only the first IMF was found to provide meaningful information about the occurrence of knock. Based on the selection criteria for the signal decomposed using EEMD, it is observed that only the first IMF needs to be analyzed further to detect the presence of knock. Similar to the EMD results, we can see two peaks in the spectrogram obtained using the first IMF at 0.01112 seconds and 0.02589 seconds, respectively. However, the energy level and frequency of the peaks are different. While comparing with the results obtained using EMD, it is also observed that, apart from the peaks observed at 0.01112 seconds and 0.02589 seconds in the first IMF, lower energy signals with a frequency above 7 kHz are found throughout the signal length in the first IMF obtained using EMD, while this was totally absent in the first IMF obtained using EEMD. This is because EEMD could extract the signals more accurately by addressing the mode mixing issue raised by EMD. Therefore, EEMD is more effective than EMD in extracting the signals produced during the occurrence of knock.

Figure 4 shows the spectrogram of the IMFs obtained by decomposing the signals using CEEMDAN. From the spectrograms, it is observed that the first and second IMFs contain signals with frequencies above 7 kHz. Similar to previous observations obtained using EMD and EEMD, two signals' energy distribution peaks were observed in the spectrogram of the first IMF at 0.01112 seconds and 0.02589 seconds, respectively. Apart from that, another peak was also observed in the spectrogram of the second IMF at 0.02589 seconds; this was totally absent in the spectrogram of IMFs obtained using EMD and EEMD. The spectrograms obtained for the first and second IMFs are required to determine the occurrence of knock in the current case. The same was also observed using the proposed selection criteria. On comparing the results obtained using EEMD and CEEMDAN, it is observed that the spectrogram corresponding to the first IMF looks alike in both cases, even though there are some changes in energy levels.

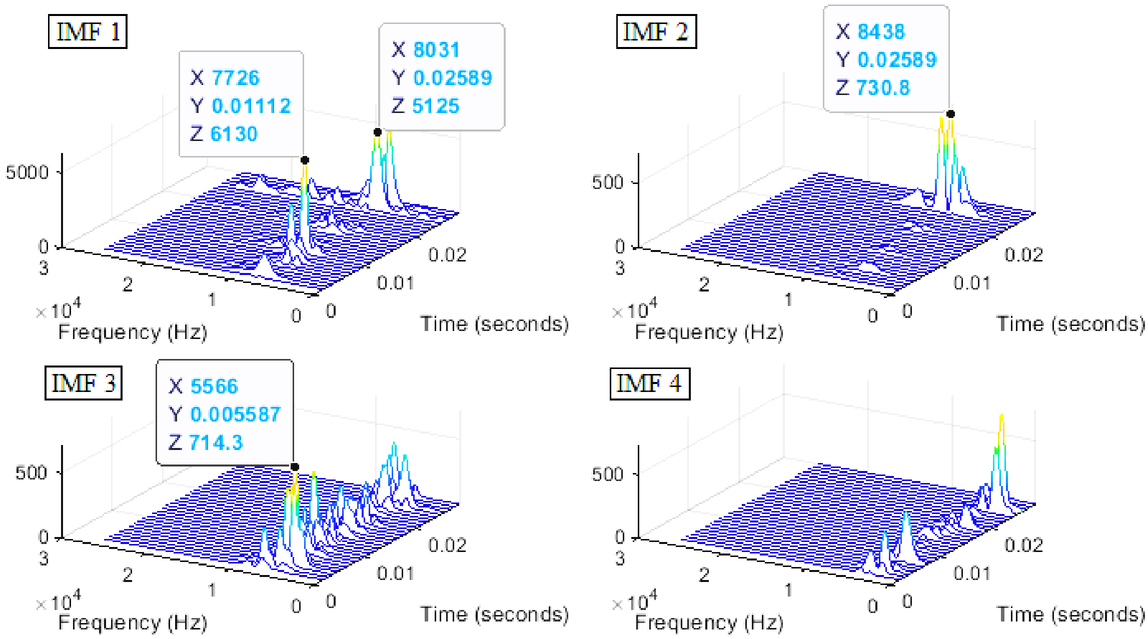

Figure 4. Spectrograms of the first four IMFs extracted using CEEMDAN from vibration signals recorded at 4000 rpm and spark at 20° BTDC

The spectrograms of the first four IMFs obtained by decomposing the signals using VMD are shown in Figure 5. The results show a different trend than those obtained using EMD, EEMD, and CEEMDAN. This is because the IMFs obtained using VMD fall in a narrow frequency band. The signals with a frequency band of 7-22 kHz were not observed in the spectrogram of the first IMF. Instead, it got distributed among the first four IMFs, i.e., knock-induced vibration signals may be distributed among the first four IMFs. The spectrograms obtained show that the energy level is mostly concentrated in the frequencies around 21 kHz, 13 kHz, 9 kHz, and 8 kHz, respectively, for the IMFs 1-4. Additionally, three peaks are observed in the spectrogram of the third IMF with frequencies around 9 kHz, but knocking was observed only at 0.01112 seconds and 0.02497 seconds, which corresponds to the combustion process in cylinders 2 and 3, as evident from the previous results obtained using EMD, EEMD, and CEEMDAN. VMD fails to identify the signals produced during the knock. This may not be the problem with the VMD method; however, it may be due to the wrong number of decomposition levels provided. Wrongly specified decomposition levels may lead to the loss of certain modes or different modes getting mixed together. Hence, extensive analysis should be done with different numbers of modes to find the optimum number of modes in which the signals need to be decomposed using VMD so that the signals produced during the knock can be clearly portrayed in one or two IMFs. The proposed selection criteria also state that VMD cannot be used effectively as EMD, EEMD, or CEEMDAN with the current number of decomposition levels provided (6).

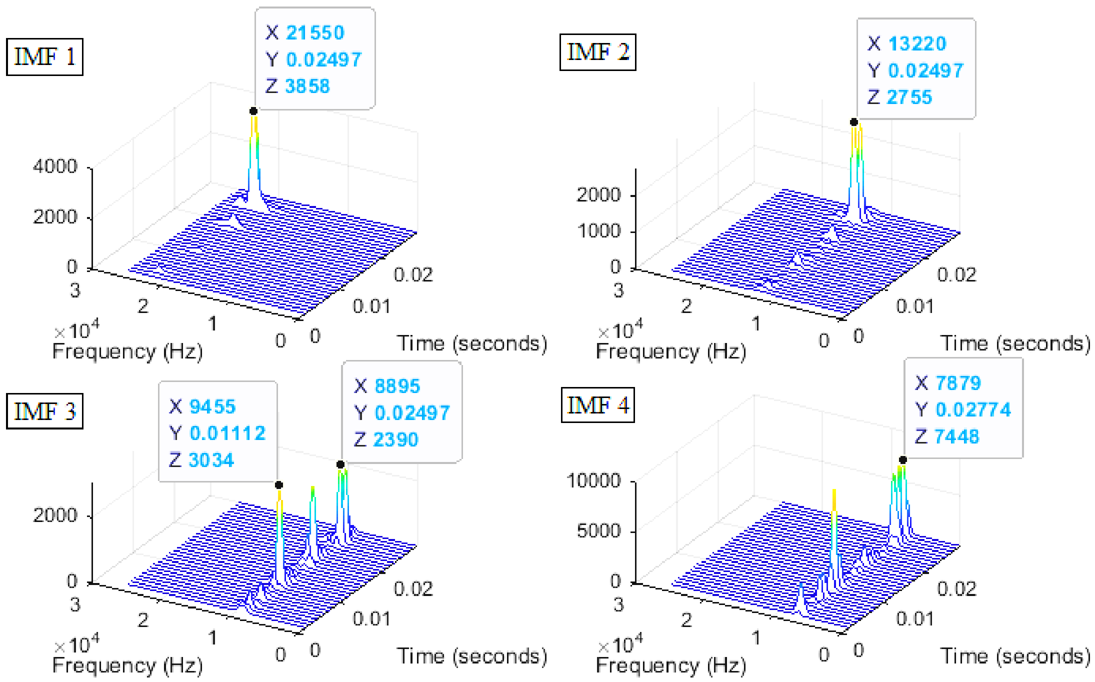

Figure 5. Spectrograms of the first four IMFs extracted using VMD from vibration signals recorded at 4000 rpm and spark at 20° BTDC

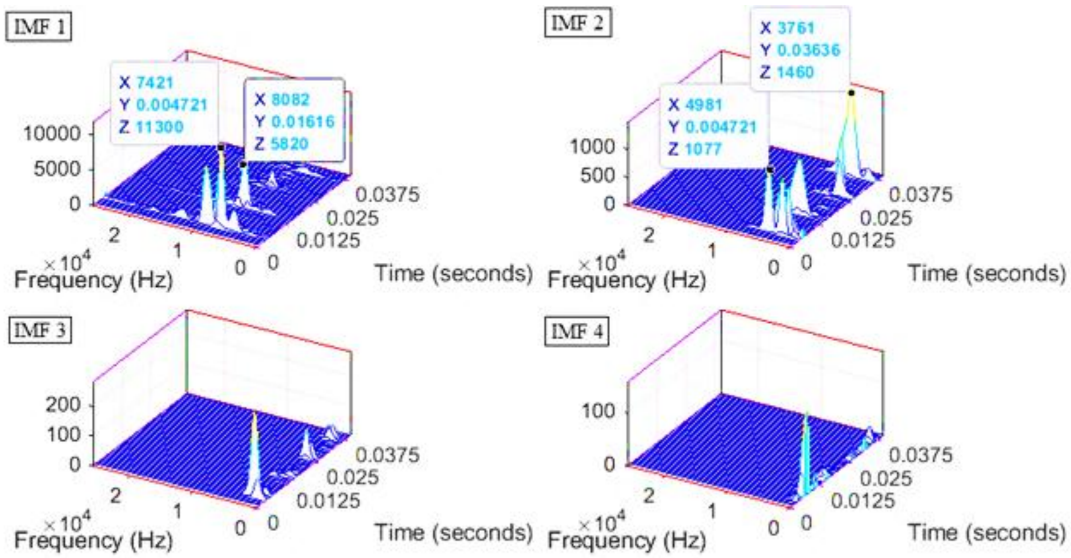

Figure 6. Spectrograms of the first four IMFs extracted using EMD from vibration signals recorded at 2800 rpm and spark at 28° BTDC

All these results show that the signals decomposed using EEMD and CEEMDAN could provide more accurate results. However, the primary focus lies in checking the feasibility of the proposed selection criterion in choosing the IMFs that may contain the signals produced during the occurrence of knock. The criterion could effectively select the IMFs that contain the signals generated during the occurrence of a knock while the engine was running at 4000 rpm and spark at 20° BTDC. The effectiveness of the same is also checked with another set of signals captured while the engine was running at 2800 rpm and spark at 28° BTDC to confirm the same.

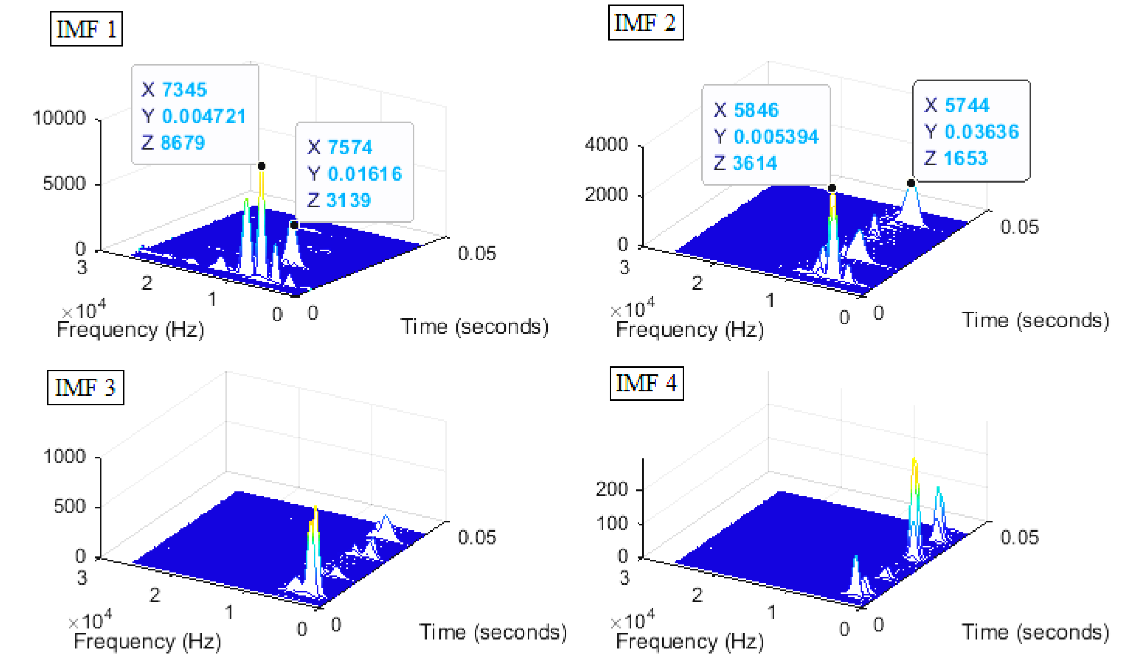

Figure 7. Spectrograms of the first four IMFs extracted using EEMD from vibration signals recorded at 2800 rpm and spark at 28° BTDC

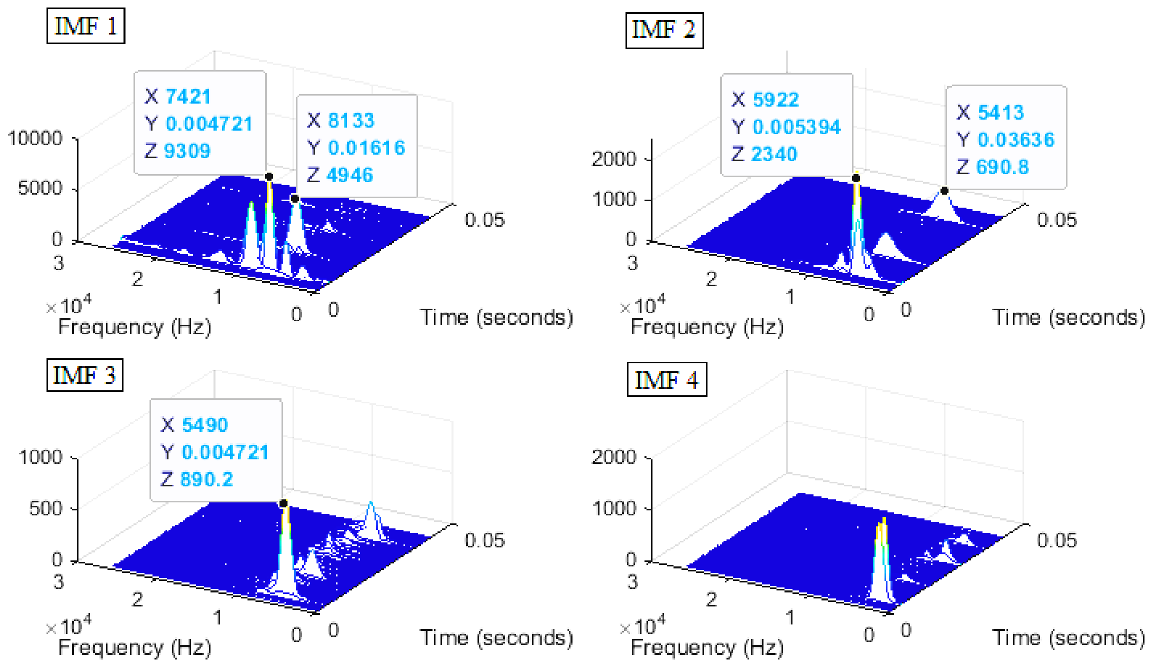

Figure 8. Spectrograms of the first four IMFs extracted using CEEMDAN from vibration signals recorded at 2800 rpm and spark at 28° BTDC

Figures 6-9 show the spectrogram of IMFs obtained by decomposing the vibration signals recorded at 2800 rpm and spark at 28° BTDC [45]. The first IMF obtained using EMD (Fig. 6), EEMD (Fig. 7), and CEEMDAN (Fig. 8) can be used to confirm the occurrence of knock, similar to the results achieved in the previous case (at 4000 rpm and spart at 20° BTDC). Two peaks at 0.0048 seconds and 0.016 seconds with frequencies around 7-8 kHz were observed in the spectrograms obtained for the first IMF using EMD, EEMD, and CEEMDAN. These timings correspond to the combustion processes inside cylinders 1 and 3. The energy level of the peak value observed at 0.004721 seconds is twice that of the energy level observed at 0.01616 seconds. This indicates a strong knock occurring in the first cylinder and a weak knock in the third cylinder. The same was also observed from the MAPO calculated. This indicates that whatever the fluctuations or disturbances in the in-cylinder pressure values are, the same will be reflected in the engine block vibrations. In Figure 8, high-frequency signals are not observed in the second IMF obtained using CEEMDAN, as observed in Figure 4. This observation is consistent with the proposed selection criteria (see Table 2). Comparing the results, it was found that the results obtained using EEMD and CEEMDAN are more efficient than those produced using

EMD. This is because, in the spectrogram corresponding to the first IMF obtained using EMD, we can observe some small peaks around 0.025 seconds and 0.0375 seconds. This was almost absent in the results obtained using EEMD, and much lower peaks were observed in the results obtained using CEEMDAN. EEMD and CEEMDAN could eliminate almost all the signals other than those produced during the occurrence of knock from the first IMF. As in the previous case, it is unable to accurately figure out the occurrence of knock using the IMFs generated by VMD with the number of levels of decomposition as 6 (Fig. 9). The signals having frequencies above 7 kHz were present in the first four IMFs obtained using VMD. Hence, VMD (with the current number of decomposition level - 6) can be ruled out from the set of decomposition techniques that can be used for determining the occurrence of knock.

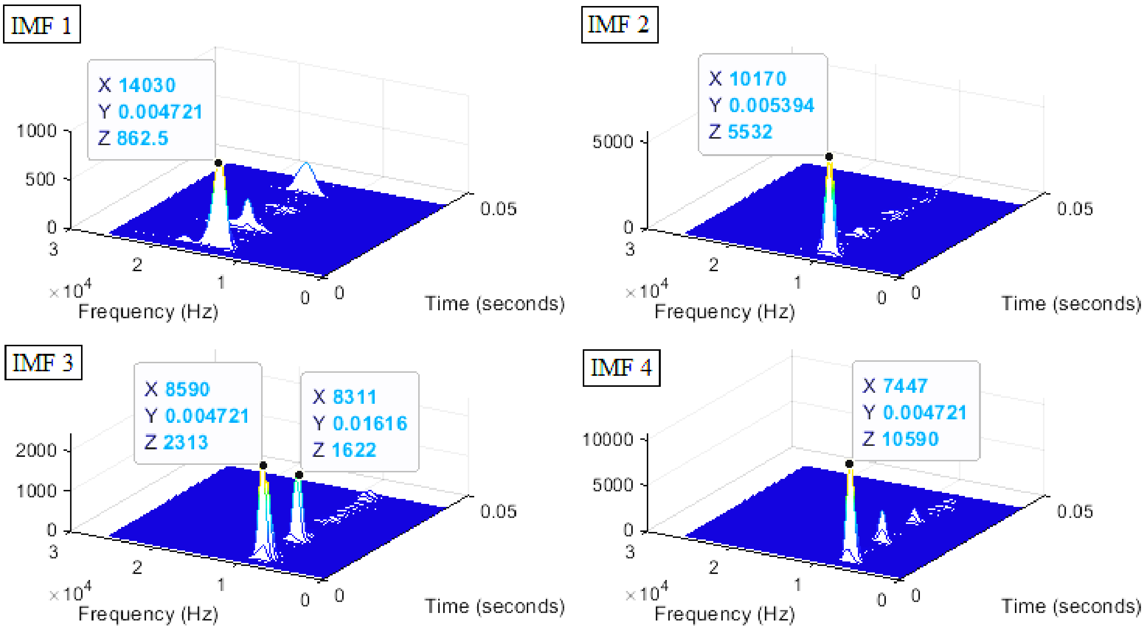

Figure 9. Spectrograms of the first four IMFs extracted using VMD from vibration signals recorded at 2800 rpm and spark at 28° BTDC

From the first and second sets of results, it is clear that the proposed selection criteria can be used to identify the IMFs that may contain the signals generated during the SI engine knock. Among the various methods used for decomposing the signal, EEMD and CEEMDAN are more efficient than EMD. At the same time, VMD is found to be inefficient in separating the high frequency, high amplitude vibrations produced during the SI engine knock from the set of engine block vibration signals. While the spectrogram analysis and statistical indicators (correlation coefficient, ApEn, and kurtosis) support the effectiveness of the proposed selection criteria, it is essential to acknowledge that the thresholds used—such as ApEn > 0.5 and correlation coefficient > 0.5—are empirically determined and may not generalize across all engine types or operating conditions. The decomposition techniques, particularly CEEMDAN and EEMD, showed promising consistency. However, their computational load remains higher than EMD, which is a challenge for real-time monitoring. The limitations observed in VMD also underscore the dependency of decomposition quality on mode number selection. These observations indicate that further optimization is required to change the parameters dynamically based on engine speed, load, and sensor characteristics for robust, real-time knock detection. Unlike prior studies that often relied on single metrics or manual IMF inspection, this work introduces a multi-parameter threshold-based selection approach that is automated, reproducible, and validated across varying speeds. Existing research, such as Bi et al. [44, 45] and Hashim et al. [23], have employed methods like Hilbert transforms or wavelet-based filtering without a structured IMF selection mechanism. The proposed method shows enhanced reliability in selecting IMFs containing knock-related features.

Furthermore, unlike previous works that relied heavily on single-feature analysis, such as kurtosis alone [39] or deep learning-based methods [36, 37] requiring substantial computational power, the current method achieves comparable knock detection accuracy while remaining computationally efficient. The approximate entropy values showed dependency on the intensity of the knock. During the occurrence of a strong knock, approximate entropy values are seen to be around 1, while during the occurrence of a weak knock, they were seen to be around 0.6. However, further extensive analysis should be done at different operating conditions to confirm its dependence. These observations also confirm the effectiveness of the proposed framework and highlight its feasibility for real-time deployment, especially when compared to the models that lack interpretability and require continuous retraining. While the current study focuses on a specific four-cylinder SI engine dataset, the methodology is designed to be adaptable to other engine types and configurations. The use of fundamental statistical features such as correlation coefficient, approximate entropy, and kurtosis, rather than engine-specific trained models, supports this generalizability. Additionally, the decomposition techniques employed (EMD, EEMD, CEEMDAN, and VMD) are widely applicable to various signal types and are not restricted to a particular engine configuration. However, it is acknowledged that optimal threshold values may vary across engines due to differences in combustion dynamics, sensor positioning, and operating ranges. Therefore, future studies should explore adaptive threshold tuning based on engine-specific characteristics, enabling broader deployment of the proposed method in research and production settings.

4. CONCLUSIONS

This study presents a systematic method for selecting knock-relevant IMFs from engine block vibration signals. The methodology involves wavelet-based denoising and decomposition using EMD, EEMD, CEEMDAN, and VMD. Each IMF is evaluated using correlation coefficient, approximate entropy, and kurtosis, and a selection criterion is applied to isolate knock-indicative components. The current work mainly focuses on the effectiveness of the proposed selection criteria in identifying the IMFs that are likely to contain the vibration signals produced during the occurrence of knock. The development of this selection criterion is based on kurtosis, approximate entropy, and correlation coefficient. Additionally, the effectiveness of various decomposition methods in extracting the signals produced during the occurrence of knock from engine block vibrations is also discussed. The comparison is made between four decomposition methods: EMD, EEMD, CEEMDAN, and VMD. The results show that EEMD and CEEMDAN outperform VMD and EMD in extracting the engine block vibration signals induced by a knock. VMD's characteristic of decomposing the signal into narrowband IMFs may not be suitable for detecting the occurrence of knock as the IMFs produced by VMD are highly dependent on the number of decomposition levels specified. EMD also fails to give accurate results due to mode mixing, where information from different oscillatory components can overlap in one IMF and may hinder the extraction of signals produced during the SI engine knock alone.

From the results, it is observed that the proposed selection criteria were able to pick the IMFs that contain the signals produced during the occurrence of knock. The spectrograms of the IMFs obtained were analyzed to confirm the same. The spectrograms of selected IMFs not only provided information regarding the presence of knock but also its intensity. This information from spectrograms was validated using MAPO. At 4000 rpm, MAPO values exceeding 2 bar and approximate entropy values approaching 1 indicated strong knock activity in cylinders 2 and 3. At the same time, MAPO corresponding to the in-cylinder pressure data obtained at 2800 rpm exceeds 4 bar corresponding to cylinder 1 and below 1.94 bar in cylinder 3, indicating strong and weak knocks, respectively. The value obtained for approximate entropy was around 0.6. Analysis should be done at different engine operating conditions to check whether this change in the value for approximate entropy directly relates to the knock intensity.

In short, for the best performance in identifying and characterizing SI engine knock using engine block vibration signals, current work recommends using either EEMD or CEEMDAN for decomposition. The subsequent selection criteria based on kurtosis, approximate entropy, and correlation coefficient can guide the selection of relevant IMFs. Additionally, extensive analysis of engine block vibration signals at various running conditions needs to be conducted to finalize the threshold values for kurtosis, approximate entropy, and correlation coefficient in order to confirm the occurrence of knock directly from the IMFs, thereby eliminating the requirement of a spectrogram. Further extensive study is required to confirm the applicability of selection criteria across different engine configurations, fuel types, and sensor locations. Adaptive tuning of these parameters based on operational profiles would enhance generalizability.

In conclusion, this work contributes a computationally efficient, statistically grounded method for knock detection using engine block vibration analysis. Future research focuses on refining threshold adaptivity, exploring ensemble learning techniques for IMF classification, and validating across diverse engine platforms to develop a deployable real-time knock control system.

ACKNOWLEDGEMENTS

This study was not supported by any grants from funding bodies in the public, private, or not-for-profit sectors.

CONFLICT OF INTEREST

The authors declare no conflicts of interest.

AUTHORS CONTRIBUTION

Antonio Joseph V K (Conceptualization; Methodology; Formal analysis; Writing - original draft)
Gireesh Kumaran Thampi (Writing - review & editing; Supervision)

REFERENCES

[1] Heywood J.B. *Internal Combustion Engine Fundamentals*, McGraw-Hill Education, 1988.

[2] Kirkpatrick, A.T. *Internal Combustion Engines: Applied Thermosciences*, John Wiley and Sons: Hoboken, NJ, USA, pp. 206–210, 2021.

[3] H. Shi, Q. Tang, K. Uddeen, B. Johansson, J. Turner, and G. Magnotti, "Effects of multiple spark ignition on engine knock under different compression ratio and fuel octane number conditions," *Fuel*, vol. 310, p. 122471, 2022.

[4] H. Shi, K. Uddeen, Y. An, and B. Johansson, "Experimental study on knock mechanism with multiple spark plugs and multiple pressure sensors," *SAE Technical Paper*, No. 2020-01-2055, 2020.

[5] D. J. Corrigan, G. Di Blasio, R. Ianniello, N. Silvestri, S. Breda, and S. Fontanesi, "Engine knock detection methods for spark ignition and prechamber combustion systems in a high-performance gasoline direct injection engine," *SAE International Journal of Engine*s, vol. 15, no. 6, pp. 883-897, 2022.

[6] Yashwanth M. Sai, T. Venugopal, and A. Ramesh, "Experimental and simulation studies to determine the effective octane number in an engine fuelled with ethanol and gasoline." *International Journal of Automotive and Mechanical Engineering*, vol. 10, pp. 2057-2069, 2014.

[7] R. Rogóż, Ł. Jan Kapusta, N. Miganakallu, Z. Yang, and J. D. Naber, "Investigation on the knock characteristics in a gasoline direct-injection engine port-injected with water-methanol blends," *Energy Conversion and Management*, vol. 258, p. 115415, 2022.

[8] Zhang Q., Pei Y., An Y., Peng Z., Qin J., Shi H., Zhang B., Zhang Z. and Gao D., "Study of water direct injection on knock control and combustion process of a high compression ratio GDI engine." *Fuel*, vol. 306, p. 121631, 2021.

[9] X. Dai, Z. Zheng, and Y. Song, "Effect of port water injection on suppressing knock in gasoline direct injection engines," *Energy Science & Engineering*, vol. 10, no. 10, pp. 3928-3945, 2022.

[10] K. Rönn, A. Swarts, V. Kalaskar, T. Alger, R. Tripathi, J. Keskiväli, et al., "Low-speed pre-ignition and super-knock in boosted spark-ignition engines: A review," *Progress in Energy and Combustion Science*, vol. 95, p. 101064, 2023.

[11] J. Kim, "Acoustic characteristics of the abnormal combustion in a high-compression ratio, spark-ignition engine," *International Journal of Automotive Technology,* vol. 23, pp. 1185–1195, 2022.

[12] J. Wang, J. Shi, J. Deng, X. Miao, Y. Liu, S. Pan, et al., "Misfire and knock detection based on the ion current inside a passive pre-chamber of gasoline engine," *Fuel,* vol. 311, p. 122528, 2022.

[13] M. Xinke, F. E. I. Shengyi, D. Jun, L. I. Liguang, H. U. Yinuo, M. A. Junjie "Simulation of charged species flow and ion current detection for knock sensing in gasoline engines with active pre-chamber," *SAE Technical Paper*, No. 2023-32-0005, 2023.

[14] H. Tajima, T. Tomidokoro, and T. Yokomori, "Deep learning for knock occurrence prediction in SI engines," *Energies*, vol. 15, p. 9315, 2022.

[15] N. Li, J. Yang, R. Zhou, and C. Liang "Determination of knock characteristics in spark ignition engines: An approach based on ensemble empirical mode decomposition," *Measurement Science and Technology*, vol. 27, no. 4, p. 045109, 2016.

[16] E. Corti, L. Raggini, A. Rossi, A. Brusa, L. Solieri, and D. Corrigan, "Application of low-cost transducers for indirect in-cylinder pressure measurements," *SAE International Journal of Engines*, vol. 16, pp. 213–230, 2023.

[17] V. Mittal, "A review of recent advancements in knock detection in spark ignition engines," *Signals*, vol. 5, no. 1, pp. 165-180, 2024.

[18] B. Pla, P. Bares, I. Jimenez, and C. Guardiola, "Increasing knock detection sensitivity by combining knock sensor signal with a control-oriented combustion model," *Mechanical Systems and Signal Processing*, vol. 168, p. 108665, 2022.

[19] S. Meng, Z. Han, B. Fan, Z. Wu, Q. Shao, and L. Tong, "Experimental study of spatial distribution of knock events in a turbocharged spark-ignition engine," *International Journal of Engine Research,* vol. 25, no. 7, pp. 1251-1264, 2024.

[20] N. Hu, H. Zhao, J. Yang, X. Zheng, H. Li, L. Xie, et al., "A knock detection method for a marine micro-ignition dual-fuel engine based on vibration signals," *Polish Maritime Research,* vol. 32, no. 1, pp. 111-120, 2025.

[21] N. E. Huang, Z. Shen, S. R. Long, M. C. Wu, H. H. Shih, Q. Zheng et al., "The empirical mode decomposition and the Hilbert spectrum for non-linear and non-stationary time series analysis," *Proceedings of the Royal Society of London. Series A: mathematical, physical and engineering sciences*, vol. 454, no. 1971, pp. 903-995, 1998.

[22] T. Q. Nguyen, T. T. D. Nguyen, H. Nguyen-Xuan, N. K. Ngo, "A correlation coefficient approach for evaluation of stiffness degradation of beams under moving load," *Computers, Materials & Continua*, vol. 61, no. 1, pp. 27-53, 2019.

[23] M. A. Hashim, M. H. Nasef, A. E. Kabeel, N. M. Ghazaly, "Combustion fault detection technique of spark ignition engine based on wavelet packet transform and artificial neural network," *Alexandria Engineering Journal*, vol. 59, no. 5, pp. 3687-3697, 2020.

[24] M. M. Ismail, M. Fawzi, J. Taweekun, and T. Leevijit, "Engine knock detection for a multifuel engine using engine block vibration with statistical approach," *MethodsX*, vol. 8, p. 101583, 2021.

[25] El Yacoubi I., and Samuel S., "Frequency coupling analysis in spark ignition engine using bispectral method and ensemble empirical mode decomposition," *SAE Technical Paper*, No. 2022-01-0481, 2022.

[26] P. Flandrin, G. Rilling, and P. Goncalves, "Empirical mode decomposition as a filter bank," *IEEE Signal Processing Letters*, vol. 11, no. 2, pp. 112-114, 2004.

[27] Z. Wu and N. E. Huang, "Ensemble empirical mode decomposition: A noise-assisted data analysis method," *Advances in adaptive data analysis*, vol. 1, no. 1, pp. 1-41, 2009.

[28] H. Han, S. Cho, S. Kwon, and S. B. Cho, "Fault diagnosis using improved complete ensemble empirical mode decomposition with adaptive noise and power-based intrinsic mode function selection algorithm," *Electronics*, vol. 7, no. 2, p. 16, 2018.

[29] M. E. Torres, M. A. Colominas, G. Schlotthauer, and P. Flandrin, "A complete ensemble empirical mode decomposition with adaptive noise," *IEEE International conference on acoustics, speech and signal processing (ICASSP)*, pp. 4144-4147, 2011.

[30] H. Purba, J. T. Musu, S. A. Diria, W. Permono, O. Sadjati, I. Sopandi, et al., "Completed ensemble empirical mode decomposition: A robust signal processing tool to identify sequence strata," In *IOP Conference Series: Earth and Environmental Science*, vol. 132, no. 1, p. 012033, 2018.

[31] J. R. Yeh, J. S. Shieh, and N. E. Huang, "Complementary ensemble empirical mode decomposition: A novel noise enhanced data analysis method," *Advances in adaptive data analysis*, vol. 2, no. 2, pp. 135-156, 2010.

[32] K. Dragomiretskiy and D. Zosso, "Variational mode decomposition," *IEEE transactions on signal processing*, vol. 62, no. 3, pp. 531-544, 2013.

[33] J. Sun, X. Zhang, Q. Tang, Y. Wang, and Y. Li, "Knock recognition of knock sensor signal based on wavelet transform and variational mode decomposition algorithm," *Energy Conversion and Management*, vol. 287, p. 117062, 2023.

[34] J. Lian, Z. Liu, H. Wang, and X. Dong, "Adaptive variational mode decomposition method for signal processing based on mode characteristic," *Mechanical Systems and Signal Processing*, vol. 107, pp. 53-77, 2018.

[35] J. Kim, "In-cylinder pressure based engine knock classification model for high-compression ratio, automotive spark-ignition engines using various signal decomposition methods," *Energies*, vol. 14, 11, p. 3117, 2021.

[36] A. B. Ofner, A .Kefalas, S. Posch, and B. C. Geiger, "Knock detection in combustion engine time series using a theory-guided 1-D convolutional neural network approach," *IEEE/ASME Transactions on Mechatronics*, vol. 27, no. 5, pp. 4101-4111, 2022.

[37] A. Kefalas, A. B. Ofner, G. Pirker, S. Posch, B. C. Geiger, and A. Wimmer, "Detection of knocking combustion using the continuous wavelet transformation and a convolutional neural network," *Energies*, vol. 14, no. 2, p. 439, 2021.

[38] J. C. M. Hernández, F. G. Madrid, H. F. Quintero, JDR Alzate, "Diesel engine diagnosis based on entropy of vibration signals and machine learning techniques," *Electronics Letters*, vol. 58, no. 11, pp. 442-444, 2022.

[39] K. M. Ramachandran and C. P. Tsokos, *Mathematical statistics with applications in R*. Academic Press, 2020.

[40] Y. He and X. Zhang, "Approximate entropy analysis of the acoustic emission from defects in rolling element bearings," *Journal of Vibration and Acoustics*, vol. 134, no. 6, p. 061012, 2012.

[41] S. L. Ding, B. Guo, Z. T. Liu, J. J. Liu, P. Tunestål, and E. Z. Song, "Analysis of the fractal characteristics for combustion instability in a premixed natural gas engine," *Applied thermal engineering*, vol. 233, p. 121177, 2023.

[42] H. Shi, K. Uddeen, Y. An, Y. Pei, and B. Johansson, "Statistical study on engine knock oscillation and heat release using multiple spark plugs and pressure sensors," *Fuel*, vol. 297, p. 120746, 2021.

[43] F. Bi, T. Ma, J. Zhang, L. Li, and C. Shi, "Knock detection in spark ignition engines base on complementary ensemble empirical mode decomposition-Hilbert transform," *Shock and Vibration*, vol. 1, p. 9507540, 2016.

[44] F. Bi, T. Ma, and J. Zhang, "Knock feature extraction in spark ignition engines using EEMD-Hilbert transform," *SAE Technical Paper*, No. 2016-01-0087, 2016.

[45] F. Bi, T. Ma, and X. Wang, "Development of a novel knock characteristic detection method for gasoline engines based on wavelet-denoising and EMD decomposition," *Mechanical Systems and Signal Processing*, vol. 117, pp. 517-536, 2019.

[46] M. A. Kabir and C. Shahnaz, "Denoising of ECG signals based on noise reduction algorithms in EMD and wavelet domains," *Biomedical Signal Processing and Control*, vol. 7, no. 5, pp. 481-489, 2012.

[47] X. Bi, J. Lin, D. Tang, F. Bi, X. Li, X. Yang, et al., "VMD-KFCM algorithm for the fault diagnosis of diesel engine vibration signals," *Energies*, vol. 13, no. 1, p. 228, 2020.

[48] M. Moradi, G. Galanopoulos, T. Kuiters, and D. Zarouchas, "A novel intelligent health indicator using acoustic waves: CEEMDAN-driven semi-supervised ensemble deep learning," *Mechanical Systems and Signal Processing*, vol. 224, p. 112156, 2025.

[49] P. A. Jargowsky and R. Yang, "Descriptive and inferential statistics," in *Encyclopedia of Social Measurement,* pp. 659-668, Elsevier Inc. 2004.

[50] S. Pincus, "Approximate entropy (ApEn) as a complexity measure," *Chaos: An Interdisciplinary Journal of Non-linear Science*, vol. 5, no. 1, pp. 110-117, 1995.